

Nanoscale studies of domain wall motion in epitaxial ferroelectric thin films

Patrycja Paruch,^{*} Thierry Giamarchi, Thomas Tybell,[†] and Jean-Marc Triscone
DPMC, University of Geneva, 24 Quai E. Ansermet, 1211 Geneva 4, Switzerland.

(Dated: July 27, 2018)

Atomic force microscopy was used to investigate ferroelectric switching and nanoscale domain dynamics in epitaxial $\text{Pb}(\text{Zr}_{0.2}\text{Ti}_{0.8})\text{O}_3$ thin films. Measurements of the writing time dependence of domain size reveal a two-step process in which nucleation is followed by radial domain growth. During this growth, the domain wall velocity exhibits a $v \propto \exp -(1/E)^\mu$ dependence on the electric field, characteristic of a creep process. The domain wall motion was analyzed both in the context of stochastic nucleation in a periodic potential as well as the canonical creep motion of an elastic manifold in a disorder potential. The dimensionality of the films suggests that disorder is at the origin of the observed domain wall creep. To investigate the effects of changing the disorder in the films, defects were introduced during crystal growth (a-axis inclusions) or by heavy ion irradiation, producing films with planar and columnar defects, respectively. The presence of these defects was found to significantly decrease the creep exponent μ , from 0.62 – 0.69 to 0.38 – 0.5 in the irradiated films and 0.19 – 0.31 in the films containing a-axis inclusions.

PACS numbers: 77.80.Fm, 77.80.Dj, 68.37.Ps, 61.80.Jh

I. INTRODUCTION

Ferroelectric materials are widely used in modern technologies in order to exploit their ferroelectric, piezoelectric and pyroelectric properties. Standard devices generally use microscopic patterned electrodes on ferroelectric ceramics, single crystals or films to produce actuators, filters, resonators, sensors and memories. However, the continuing demand for miniaturization in acoustic applications [1], in ultra-high density information storage [2, 3], and in micro-electro-mechanical systems (MEMS), has made alternative solutions necessary. In terms of material growth, techniques like rf-magnetron sputtering, pulsed laser deposition, and molecular beam epitaxy with in-situ characterization [4] have been developed to precisely control the structure and thickness of materials. Today, these techniques allow epitaxial thin films with atomically flat surfaces and interfaces to be grown, both in all-oxide structures and, more recently, on top of silicon [5]. Combined with these techniques, increased understanding and control of oxide growth modes has permitted self-assembly processes and nanostructuring in single crystals and thin films [6], a novel approach to miniaturization. Low-temperature metallo-organic chemical vapor deposition, more easily adaptable to industrial applications, has also been actively researched to produce uniform films over large areas with low fatigue [7]. As device dimensions become reduced in extremely miniaturized systems, an important issue is the ability to locally access and control ferroelectricity. From its inception, there has been significant interest in using atomic force microscopy (AFM) [8, 9, 10] for this purpose, since

it allows control over ferroelectric domain structure at the nanoscopic scale required by ever smaller systems. For such systems, ferroelectric domain stability, domain dynamics in the presence of electric fields or temperature variations, and issues of domain growth are the main concerns. Therefore, understanding the fundamental physics of ferroelectric domains in thin films is of crucial importance.

In this respect, it is useful to consider domain walls in ferroelectric materials within the broader framework of elastic disordered systems in the presence of an external force. Indeed, ferroelectric materials are characterized by energetically equivalent, degenerate ground states (tetragonal, in the case of the perovskite materials used in this study), separated by an energy barrier. In a ferroelectric ground state the center of gravity of positive charge in the unit cell is displaced relative to the center of gravity of the negative charge, leading to a stable remanent polarization reversible under an electric field, as shown schematically in Fig. 1. Regions of opposite polarization are separated by thin interfaces, or domain walls. The application of an electric field asymmetrizes the ferroelectric double well potential, favoring one polarization state over the other by reducing the energy necessary to create a nucleus with polarization anti-parallel to the field, thus promoting domain wall motion. These domain walls can be considered as elastic objects, whose surface tends to be minimized in order to decrease the total wall energy. However, such elastic objects may meander from an optimal flat configuration in order to take advantage of particularly favorable regions of the potential landscape, which can vary due to disorder in the ferroelectric film, as well as the commensurate potential of the crystal lattice itself. The behavior of such systems is thus governed by the competition between elasticity and the effects of pinning. Although at $T = 0$ the domain wall is pinned by the disorder until a critical force f_c is reached, at finite temperatures it can be driven by forces below

^{*}Electronic address: patrycja.paruch@physics.unige.ch

[†]Now at Department of Electronics and Telecommunications, Norwegian University of Science and Technology, N-7491 Trondheim, Norway.

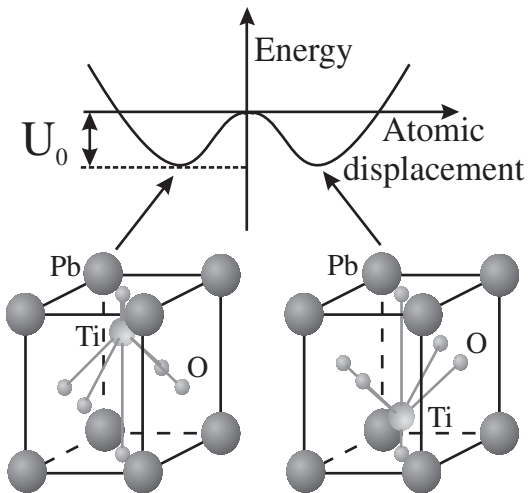


FIG. 1: Schematic diagram of a $\text{Pb}(\text{Zr}_{0.2}\text{Ti}_{0.8})\text{O}_3$ unit cell in two degenerate ground states separated by an energy barrier U_0 . The Pb and Ti/Zr ions are positively charged and the O ions are negatively charged, giving opposite polarization directions P_{DOWN} and P_{UP} .

f_c , since barriers to motion, however high, can always be passed via thermal activation. How the domain wall moves when driven at small forces is of theoretical and practical interest. A simple answer [11] is motion governed by a linear response of the form $v \propto e^{-\beta\Delta} f$ due to thermal activation above pinning barriers Δ , where β is the inverse temperature $1/k_B T$ and $f \ll f_c$ is the driving force. However, subsequent detailed analysis showed that both periodic [12, 13] and disordered pinning potentials [14, 15, 16] can lead to diverging barriers and thus to a nonlinear “creep” response, in which the velocity is, for small temperatures and for forces much smaller than the critical force, of the form $v \propto \exp(-\beta U_c (f_c/f)^\mu)$. U_c is a barrier height and μ is an exponent characteristic of the mechanism responsible for the creep. In a periodic potential creep occurs only for interfaces of dimension $d = 2$ (sheets), and $\mu = 1$ [13]. For creep in a random potential $\mu = (d - 2 + 2\zeta)/(2 - \zeta)$, where d is the dimensionality of the interface and ζ its equilibrium roughness exponent (see Section V). Note that the nature of the disorder only enters through the static roughness exponent ζ . Measurements of domain wall motion and equilibrium roughness configuration in ultrathin magnetic films have verified the creep law prediction for interfaces, with the measured exponent $\mu = 0.25$ in good agreement with the expected theoretical values for this system [17]. In periodic vortex systems, precise determination of the exponents has been complicated by the multiple scales of the problem [13, 18], although results in agreement with the theoretical predictions of $\zeta = 0$ have been observed [19]. High quality epitaxial ferroelectric thin films are therefore another interesting model system to study such phenomena, because their thickness and crystalline quality can be precisely controlled, and because AFM allows nanometer resolution of their domain configuration.

In this paper, we present a review of our studies of non-invasive, local AFM control of ferroelectric polarization in epitaxial $\text{Pb}(\text{Zr}_{0.2}\text{Ti}_{0.8})\text{O}_3$ (PZT) thin films and its possible applications. We will focus specifically on the behavior of domain walls and its relation to domain growth and stability. We expand on the discussion of our previous results demonstrating that domain wall motion in thin films is a disorder-controlled creep process. In particular, we discuss the differences between the usual stochastic nucleation scenario proposed by Miller and Weinreich to explain domain wall motion observed in bulk ferroelectrics [12], and the creep scenario due to the competition between a disorder potential and the elasticity of the wall. Finally, we report on new studies of ferroelectric materials in which domain dynamics are measured in the presence of macroscopic defects, both columnar, in the form of heavy ion irradiation tracks, and planar, in the form of a-axis inclusions in the c-axis oriented films. We find that these defects, macroscopic in relation to the thickness of the domain wall, nonetheless have a significant effect on domain wall dynamics, lowering the values of the critical exponent for domain wall creep from 0.62 – 0.69 to 0.38 – 0.5 in irradiated films, and down to 0.19 – 0.31 in films containing a-axis inclusions [20].

II. THIN FILM FABRICATION AND AFM WRITING

The ferroelectric materials used in this study were c-axis oriented PZT thin films, epitaxially grown by off-axis rf-magnetron sputtering onto conductive (0.5 % wt) Nb:SrTiO₃ (001) substrates in an Ar:O₂ flow at 180 mTorr, and at substrate temperatures of $\sim 500^\circ\text{C}$. Multiple samples with thicknesses varying from 29.0 to 130.0 nm were grown. X-ray characterization of the films, such as the θ - 2θ diffractogram shown in Fig. 2, revealed high crystalline quality, with ϕ scans (not shown) confirming epitaxial “cube-on-cube” growth of the ferroelectric material on the substrate. The multiple orders of satellite reflections around the principal 001 PZT peak are due to the finite size of the sample, and allow us to precisely determine the thickness of the films. Measurements of sample topography showed uniform surfaces with root-mean-square (rms) roughness of 0.2 – 0.3 nm over $5 \times 5 \mu\text{m}$ areas as shown in Fig. 3, where the vertical scale is equal to 1 % of the 54 nm thickness of the film itself. High crystalline quality and smooth surfaces are advantageous for effective writing and imaging of ferroelectric domains, since the presence of morphological defects could perturb the tip-sample interaction and thereby complicate the use of the films as model systems for domain wall studies.

To locally control the ferroelectric polarization state, a metallic AFM tip was used as a mobile top electrode, while the conductive substrate functioned as a bottom electrode. Applying a voltage between the tip and the substrate results in a local electric field across the fer-

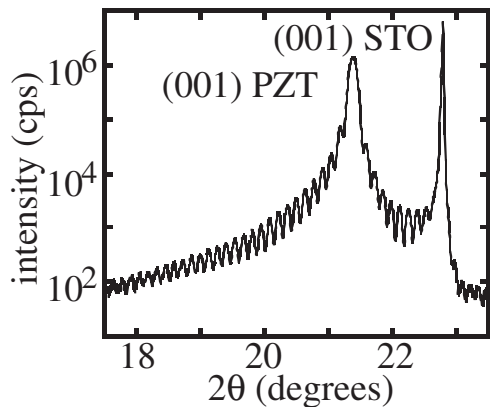


FIG. 2: θ - 2θ scan of the PZT 001 peak in a 50 nm epitaxial thin film. Multiple orders of finite size reflections allow precise measurement of film thickness.

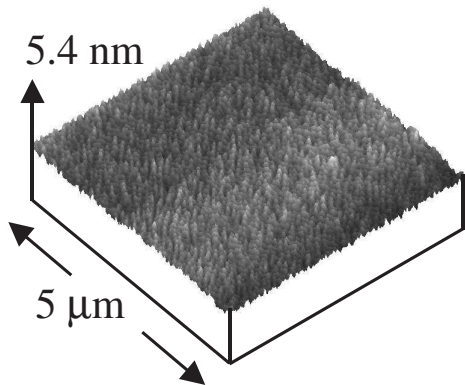


FIG. 3: AFM topography of a 54 nm PZT film showing 0.22 nm rms roughness over a $5 \times 5 \mu\text{m}^2$ area.

roelectric thin film, favoring the polarization direction parallel to the field. This leads to polarization switching if the field is high enough (or applied for long times), as shown schematically in Fig. 4. To image the resulting domains the phase contrast of the local piezoresponse of the film, excited by the application of a small oscillating voltage via the AFM tip, (detailed in Fig. 5) is measured by piezo-force microscopy (PFM). All measurements were performed on commercially available *Veeco Multimode* equipment.

Large areas, essentially limited only by the scan area of the AFM and ultimately, the size of the sample itself, can be polarized by applying a constant voltage to a tip scanning in contact with the surface [9]. One can also alternate positive and negative voltages applied for a fixed duration with respect to the scanning speed of the sample to create arrays of lines with opposite polarization, such as those shown in Fig. 6, where the line width is 925 ± 15 nm. Such linear domain structures have been used to develop a new type of interdigitated transducer for a prototype high-frequency surface acoustic wave device [21]. Frequencies up to 3.4 GHz have

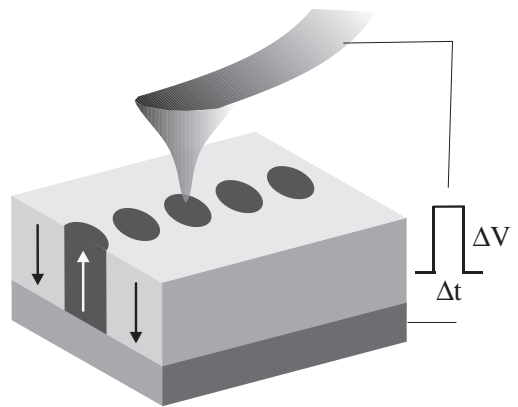


FIG. 4: Schematic representation of local polarization switching in a ferroelectric thin film. The application of voltage pulses of magnitude ΔV and duration Δt between a metallic AFM tip and the conducting substrate produces nanoscale circular domains penetrating through the thickness of the film.

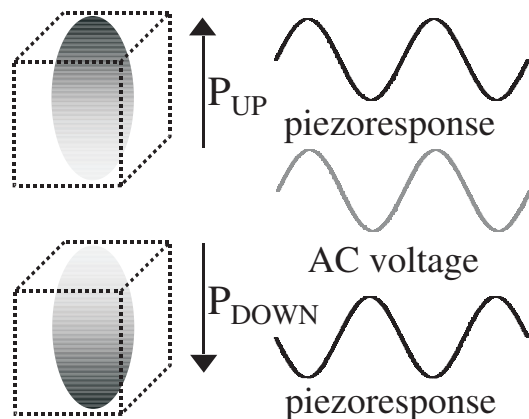


FIG. 5: Schematic representation of the two antisymmetric polarization states in the tetragonal ferroelectric PZT unit cell. Applying a small AC voltage with an AFM tip excites a local piezoresponse, detected using a lock-in technique. The two polarization states (P_{UP} and P_{DOWN} .) respond 180° out of phase with each other, thus allowing a phase contrast image of the ferroelectric domains to be obtained.

been demonstrated, but higher frequencies are in principle readily accessible since AFM writing allows very small line widths. For instance, using carbon nanotube bundles attached to a metallic AFM tip to achieve a very high aspect ratio, we were able to write a network of lines as small as 20-30 nm [22]. Small circular domains can also be created by applying short voltage pulses to a stationary tip in contact with the sample, at desired positions in a uniformly prepolarized area. As we have previously shown, such domains can be written in arrays with densities as high as $\sim 30\text{Gbit}/\text{cm}^2$, with each domain (bit) in such an array individually accessible and fully reversible under subsequent voltage pulses [23], an important consideration from the point of view of dynamic non-volatile memory applications. Subsequently, Cho *et*

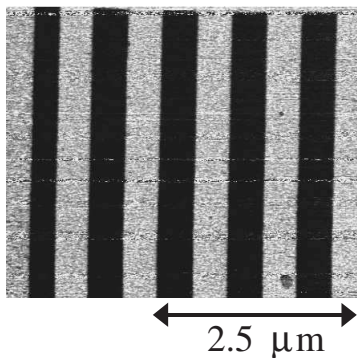


FIG. 6: PFM image of AFM-written linear ferroelectric domains 925 ± 15 nm wide. Similar domain structures have been used in a prototype surface acoustic wave device with GHz frequencies.

al. have demonstrated individual domains ~ 15 nm in diameter in ferroelectric single crystals which would give densities as high as 0.5 Tbit/cm² [24] when projected into a standard array. By identifying the parameters controlling domain size as the writing time and writing voltage (the duration and magnitude, respectively, of the voltage pulse applied to create the domain), and the confinement of the electric field at the AFM tip our studies address an active area of interest for ferroelectric non-volatile memories: how to achieve the required ultrahigh information densities.

Two other key issues for information storage applications are the minimum switching time and the stability of the resulting domains. Using the AFM, we have written domains with pulses as short as 5 ns, with radii of 18.5 ± 4 nm. This is not a fundamental limit, however, but rather an experimental consideration related to the minimum pulse time achieved by our pulse generator and the RC characteristics of our system, which may lead to distortion of the applied pulse at very short times. Recent studies by Li *et al.* using a photoconductive switch and femtosecond laser illumination suggest that the actual switching time for ferroelectric domains may be as short as $\sim 70 - 90$ ps [25]. Our studies have also consistently shown very high stability of AFM-written ferroelectric domains. An array of 16 domains written with 500 ns pulses was imaged immediately after writing (Fig. 7(a)), showing well defined homogeneous domains with regular spacing and radii of 29.2 ± 4 nm. The array was followed with measurements performed at 1 week (Fig. 7(b)), 2 weeks (Fig. 7(c)) and 1 month (Fig. 7(d)), with radii of 27.0 ± 4 nm, 27.2 ± 4 nm and 27.7 ± 4 nm respectively. No change, backswitching, or spontaneous disappearance of the domains were observed. Additionally, the arrays of lines used for surface acoustic wave devices were measured over a period of 4 months, after lithographic patterning, etching of areas outside the filter region, and the application of voltage signals larger than those used for the piezoelectric response in order to excite surface acoustic waves. Once again, the domain structures remained

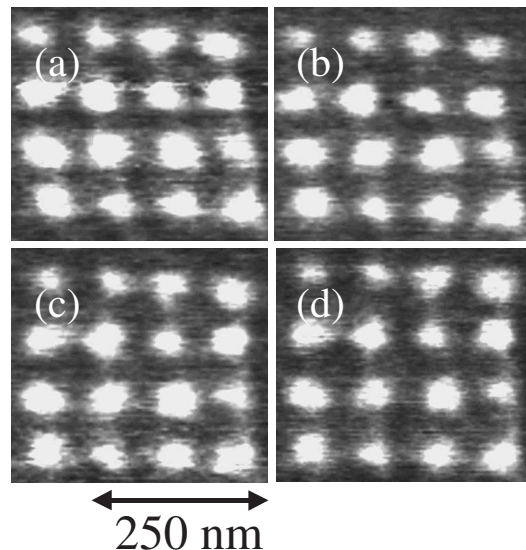


FIG. 7: PFM images of the same array written with 500 ns, 12 V pulses, straight after writing (a), 1 week later (b), after 2 weeks (c) and at the end of the experiment, a month later (d). The average domain radii are 29.2 nm, 27.0 nm, 27.2 nm and 27.7 nm respectively, unchanged within the ± 4 nm error of the experiment.

completely stable [21]. Moreover, similar linear domains heated to 440°C did not show any change when imaged after subsequent cooling [26]. It is therefore likely that pre-written ferroelectric domain structures in thin films can subsequently be incorporated into further processing steps up to, and possibly well beyond this temperature. As shall be explained in more detail, such high stability in zero applied field is in fact inherent to the glassy behavior of an elastic disordered system.

III. EXPERIMENTAL OBSERVATION OF DOMAIN WALL CREEP

The local control of ferroelectric polarization provided by AFM, together with its nanometer resolution, also make it a powerful tool for fundamental studies of domain dynamics and dependence on writing parameters such as the writing time. As previously reported [23], we observed a strong dependence of domain radius on the writing time for times longer than $\sim 20 \mu\text{s}$. For shorter times, domain radii appeared to saturate at ~ 20 nm, a size we relate to the 25 – 50 nm nominal radius of curvature of the AFM tip used for these experiments. For each writing time, 16- or 25-domain arrays were written with 12 V pulses, and the domain radius was calculated by averaging over the measured domain radii along their vertical and horizontal axes, with a rms error of $\sim 10\%$. All imaged domains appeared homogeneous and well defined and no randomly nucleated domains were observed. These data suggest a two-step switching process: first, rapid nucleation and forward growth across

the thickness of the sample occur under the AFM tip; this event is followed by slower radial motion of the domain wall outwards, perpendicular to the polarization direction, in order to increase domain size. We analyzed this radial domain wall motion in the framework of a pinned elastic system by comparing the velocity and the driving force exerted on the wall, in our case due to the electric field E applied by the tip. We considered arrays written with consecutive pulse durations, extracting the domain wall velocity as $v = \frac{r(t_2) - r(t_1)}{t_2 - t_1}$, the difference in domain radii at the two subsequent writing times divided by the difference in the writing times themselves. The electric field distribution was obtained by modelling the tip as a charged sphere, with radius α taken as equal to the domain saturation size of 20 nm. Applying a voltage V to the tip at the surface of the ferroelectric film with dielectric constant ϵ produces a charge $q = 4\pi\epsilon\epsilon_0\alpha V$ on the model tip. Taking into account both the effect of the film and the conductive substrate, we are able to find the field $E_{\perp}(r, z)$ at any point (r, z) within the film. r is the horizontal distance (in the plane of the film) away from the center of the spherical tip, and z is the depth within the film (up to thickness λ) from the center of the tip. In our experiments, the domain radii remain comparable to the size of the tip, so further simplification can be obtained by considering only the first order of image charge reflections in the film and the substrate. Since the voltage drop V across the film is simply the integral of this field over the film thickness $V = \int_0^{\alpha+\lambda} E_{\perp}(r, z) dz$ we can define the average field across the film $E(r) = \overline{E_{\perp}}(r)$, which shows a $1/r$ dependence in this first order approximation. As one moves further away from the tip, a crossover to higher orders of r dependence in the denominator is expected for the field. This simplified model shows reasonable agreement with a more accurate numerical simulation of a hyperbolic tip in contact with a ferroelectric film grown on a metallic substrate. Here, a $1/r$ dependence of the electric field is observed out to $r \sim 150$ nm, for a tip $1 \mu\text{m}$ high with $\alpha = 20$ nm radius of curvature. Beyond this, a cross over to $1/r^2$ and even steeper field decay occurs.

Although the field $E(r)$ is highly inhomogeneous at large length scales, it can be taken as constant over the very small thickness (on the order of a lattice spacing) of the ferroelectric domain wall. One can thus relate the velocity $v(r)$ of the domain wall at a distance r from the tip to a field $E(r) = \frac{V\alpha}{r\lambda}$, where $r = \frac{r(t_1) + r(t_2)}{2}$. An Arrhenius plot of the velocity against the inverse field, shown in Fig. 8, reveals that our data are in good agreement with a creep behavior

$$v \sim \exp - \frac{U_c}{k_B T} \left(\frac{E_0}{E} \right)^{\mu} \quad (1)$$

over multiple decades of velocity, from 10^{-3} to 10^{-9} m/s, and for fields varying from 10^7 to 5×10^8 V/m [48]. The values of the dynamical exponent μ were found to be close to 1 for the original three samples [27], and closer to 0.7 for seven later samples – grown and measured under the

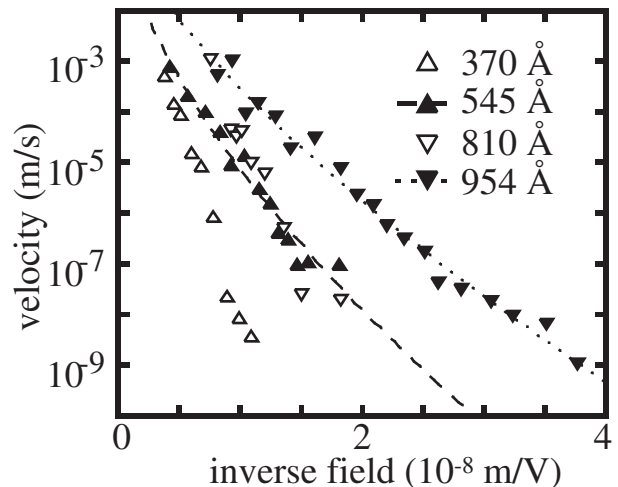


FIG. 8: Domain wall speed as a function of the inverse applied electric field for 37.0, 54.5, 81.0 and 95.4 nm thick films. The data agree with the creep equation $v \sim \exp[-\frac{R}{k_B T} (\frac{E_0}{E})^{\mu}]$ with $\mu = 0.93, 0.62, 1.19,$ and 0.70 respectively. Fits of the data to $\log v = A(1/E)^{\mu}$ are shown for the 54.5 and 95.4 nm films.

same conditions. These data were the first indication that domain wall motion in ferroelectric thin films was a creep process, and led us to investigate its microscopic origins.

IV. DOMAIN WALL CREEP IN A COMMENSURATE POTENTIAL

Early studies [28, 29] of domain growth carried out by optical and etching techniques on bulk samples reported a non-linear electric field dependence of the velocity $v \propto \exp -1/E$ known as Merz's law (with implicit values of $\mu = 1$, if these results are to be considered in the general framework of creep). At the time, a phenomenological theory based on the stochastic nucleation of new domains at existing domain boundaries was put forward by Miller and Weinreich to explain the observed behavior [12]. The wall moves forward due to the formation of a nucleus as shown in Fig. 9. The energy change due to the formation of a nucleus is

$$\Delta F = -2P_s E V + \sigma_w A + U_{\text{depolarization}} \quad (2)$$

Nucleation would occur and the domain wall would move if the energy gain, due to switching a volume V of ferroelectric with spontaneous polarization P_s to the polarization state energetically favorable with respect to the direction of the applied field E , would balance the energy cost of extending the surface A of the domain wall, with a surface energy density of σ_w , as well as the incurred depolarization energy cost $U_{\text{depolarization}}$. In fact, this mechanism is identical [49] to the one of an elastic manifold weakly driven in a periodic pinning potential

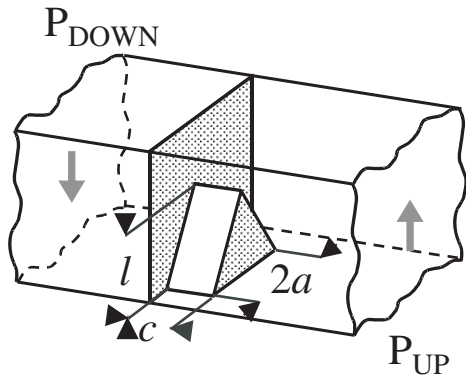


FIG. 9: Schematic drawing of a triangular step domain on a 180° domain wall, as described by Miller and Weinreich [12]. The applied electric field E is parallel to P_{DOWN} .

(tilted washboard potential, as described for example in [13]). The nucleus thickness (c in Fig. 9) is the distance between two minima of the periodic potential given by the lattice spacing of the ferroelectric crystal.

For small electric fields ($E \rightarrow 0$) a large nucleus can be expected since the energy gain due to the displacement of a nucleus into the neighboring pinning valley grows with the volume of the nucleus, while the energy cost essentially scales with its surface. Since $V \sim L^d$ while $A \sim L^{d-1}$, where L is the extension of the nucleus, and d the dimensionality of the elastic interface, two cases occur. For a one-dimensional manifold (string, $d = 1$), the nucleus consists of two point-like kinks, whose activation energy therefore always remains finite, and the system exhibits a *linear* response under small driving forces. For a two dimensional manifold, on the other hand, minimizing (2) gives $L^* \sim 1/E$, showing that the size of the nucleus grows as the electric field decreases. The energy barriers the nucleus has to overcome thus grow as $\Delta(E) \sim 1/E$, using (2), giving a non-linear response with $v \propto \exp -1/E$. The stochastic nucleation scenario proposed by Miller and Weinreich can thus explain the observed non-linear response of the domain wall *only if* the domain wall itself is a two-dimensional surface embedded in a three-dimensional crystal. This means that the dimensions of the nucleus, at a given field E , have to be smaller than the thickness of the system. Otherwise, the energy of the nucleus saturates and the one dimensional wall case and a linear response are recovered. It is also important to note that if the creep consists of motion in a periodic potential the creep exponent is constrained to be $\mu = 1$. As already mentioned, this particular scenario is microscopically related to the intrinsic periodic potential of the ferroelectric crystal itself acting to pin the domain wall. The strength of this potential was calculated in *ab-initio* studies of 180° domain walls in PbTiO_3 , showing that the wall energy varies from 132 mJ/m^2 to 169 mJ/m^2 depending on whether the domain wall is centered on a Pb-O or Ti-O₂ plane in the crystal

[30]. The influence of such a periodic potential is due to the extreme thinness of the domain wall in ferroelectric materials, in contrast to magnetic systems where the domain wall is much larger than the atomic length scales [17].

In order to test whether the observed creep behavior is indeed due to the nucleation process, we calculated the size of the critical nucleus, following the formulation derived by Miller and Weinreich for the energetically most favorable dagger-shaped nucleus of horizontal extension a , height l and thickness c forming at an existing 180° domain wall, as shown in Fig 9 [12], where P_s is the polarization, b the in plane lattice constant, ϵ the dielectric constant of PZT at ambient conditions, and E the applied electric field. The depolarization energy can be written as $U_{\text{depolarization}} = \frac{2\sigma_p b a^2}{l}$, with $\sigma_p = (4P_s^2 b \ln(0.7358a/b))/\epsilon$ [12]. By minimizing the free energy change due to nucleation with respect to the dimensions of the nucleus a and l , with c taken as equivalent to the lattice constant b (the distance between two minima in the periodic crystalline potential), the size of the critical nucleus a^* and l^* , as well as the activation energy ΔF^* , can be calculated as [12]:

$$\begin{aligned} a^* &= \frac{\sigma_w(\sigma_w + 2\sigma_p)}{P_s E(\sigma_w + 3\sigma_p)} \\ l^* &= \frac{\sigma_w^{1/2}(\sigma_w + 2\sigma_p)}{P_s E(\sigma_w + 3\sigma_p)^{1/2}} \\ \Delta F^* &= \frac{4b}{P_s E} \sigma_p (\sigma_w + 2\sigma_p) \left(\frac{\sigma_w}{\sigma_w + 3\sigma_p} \right)^{3/2} \end{aligned} \quad (3)$$

To compute the actual values, we take the standard parameters for PZT ($P_s = 0.40 \text{ C/m}^2$, $\epsilon = 100$, $b = 3.96 \text{ \AA}$), and the *ab-initio* value for the domain wall energy density [50] $\sigma_w = 0.132 \text{ mJ/m}^2$. In our case, the applied electric field varied from ~ 2 to 20 MV/m (with the factor 10 correction), depending on the thickness of the sample used and the distance from the AFM tip, with the most intense fields for thin films and small domains. Corresponding values of σ_p were between 1.6 and 0.9 J/m^2 . Since σ_p is therefore greater than σ_w , following Miller and Weinreich, the expressions for the critical values can be simplified to:

$$\begin{aligned} a^* &= \frac{2}{3} \frac{\sigma_w}{P_s E} \\ l^* &= \frac{2\sigma_w^{1/2} \sigma_p^{1/2}}{\sqrt{3} P_s E} \\ \Delta F^* &= \frac{8b}{3\sqrt{3} P_s E} \sigma_p^{1/2} \sigma_w^{3/2} \end{aligned} \quad (4)$$

For the field range used, these equations would give critical values of $a^* \sim 12.5 - 125 \text{ nm}$ and $l^* \sim 53 - 710 \text{ nm}$. These results imply that for the given value of field, the vertical size of the critical nucleus would exceed the thickness of the film itself. This suggests that the films are in a 2-dimensional limit, with the domain walls acting as a

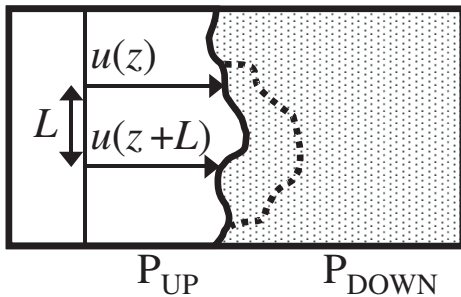


FIG. 10: Domain wall as elastic manifold trapped in a random disorder potential. In equilibrium, the domain wall exhibits a characteristic roughness, measured by the correlation function $B(z) = \langle [u(z+L) - u(z)]^2 \rangle$ of the displacements $u(z)$ from elastically ideal flat configuration with respect to the length L of domain wall. In the presence of a small driving force $f < f_c$ due to the applied electric field E , the domain wall will move to the next favorable configuration in the disorder potential, as shown by the dotted line, via a glassy creep motion.

quasi-one-dimensional manifold, for which the Miller and Weinreich stochastic nucleation model, or alternatively, weakly driven motion through a periodic potential, could not explain the non-linear response observed. Finally, the values of the dynamical exponent we observe, generally not equal to one, are also a strong indication that an alternative microscopic mechanism for the observed creep process should be considered.

V. DOMAIN WALL CREEP IN A RANDOM POTENTIAL

In the alternative scenario of a canonical “glassy” system, an elastic manifold is weakly collectively pinned by the quenched disorder potential present in the medium, with important consequences for both its static and dynamic behavior. Since disorder is always present in any realistic system it is a feasible source of the observed domain wall creep in ferroelectric thin films. Both for vortices in superconductors [13] and in magnetic systems [17], disorder is clearly the driving mechanism behind the observed creep behavior. In PZT, a solid solution of 20% PbZrO_3 in 80% PbTiO_3 , the presence of Zr atoms is a possible source of disorder, although preliminary studies of domain wall dynamics in pure PbTiO_3 show similar behaviour to that observed in PZT. Vacancies and other defects in the lattice structure are also likely sources of disorder. In ferroelectric films the presence of disorder would dominate domain wall behaviour for both one and 2 dimensional walls at large scales. However, given the thinness of the domain wall, we note that the periodic potential of the crystal is also present in the problem. In principle, ferroelectric films could therefore ultimately be used to study the competition between a periodic potential and disorder (see e.g. [31]).

In order to analyze the effects of disorder on domain wall motion let us again consider the energy for a segment of ferroelectric domain wall of length L displaced by $u(z)$ from the elastically ideal flat configuration (where z are the internal coordinates, such that the total spatial dimension $d = z + 1$), as shown on Fig. 10. The energy scales as[51]

$$U(u, L) = \sigma_w u^2 L^{d-2} - U_{\text{disorder}}[u] - 2P_s E L^d u \quad (5)$$

where the first term describes the elastic energy contribution, and is expressed for a local elasticity [52]. A more accurate description of long range forces, such as dipolar forces, modifies the elasticity and amounts to replacing d by $(3d - 1)/2$ in the following formulas(see e.g. [31] and ref. therein). The second term is due to pinning by the disorder potential, and the third is the energy due to the application of an external electric field. $U_{\text{dis.}}$ depends on the precise nature of the disorder. For example for “random bond” disorder, equivalent to defects which locally modify the ferroelectric double well potential depth, one can model the disorder by a random potential acting at the position of the interface and

$$U_{\text{disorder}} = \int d^d z V(u(z), z) \quad (6)$$

Another form of disorder, the so called “random field”, occurs when defects locally asymmetricize the ferroelectric double well potential, leading to a different form for $E_{\text{dis.}}$. If the disorder is weak, the central limit theorem allows its approximation by a Gaussian random potential. The disorder is then only characterized by its correlation length r_f and the strength of the random potential. In the absence of an external electric field, the configuration of the domain wall results from the competition between the elastic forces and the random potential. This configuration can be characterized by measuring the correlation function of relative displacements

$$B(L) = \overline{\langle [u(z+L) - u(z)]^2 \rangle} = \xi^2 \left(\frac{L}{L_c} \right)^{2\zeta} \quad (7)$$

where $\langle \dots \rangle$ denotes thermal averaging (thermodynamic equilibrium) and $\overline{\dots}$ denotes an ensemble average over the realization of the disorder. In a realistic experimental situation the ensemble average is performed by averaging over all pairs of points separated by a distance L , assuming that the system is self-averaging. $B(L)$ shows a power-law growth with different exponents. For r smaller than a characteristic length, the Larkin length L_c [32, 33], $B(L)$ grows as $B(L) \sim L^{4-d}$. Below this length there is no metastability and no pinning of the elastic interface. Above the Larkin length, the growth still follows a power law, but with an exponent 2ζ ($B(L) \sim L^{2\zeta}$) dependent on the nature of the disorder. The Larkin length corresponds to the length for which the displacements are of the order of the size of the interface or the correlation length of the random potential [53] $B(L_c) = \max(\xi, r_f)$.

The Larkin length is thus the smallest length at which the wall can be weakly pinned, and above which it can adjust elastically to optimize its local configuration [54]. Above R_c one can thus write

$$B(L > L_c) = \max(\xi, r_f)^2 \left(\frac{L}{L_c}\right)^{2\zeta} \quad (8)$$

The roughness exponent ζ is a function of the type of disorder present in the film, and the dimensionality of the manifold. For a line ($d = 1$) and purely thermal fluctuations in the absence of disorder, $\zeta = 0.5$. In a random bond scenario, an exact value of $\zeta = 2/3$ has been calculated for a line [34, 35, 36] and $\zeta \sim 3/5$ [37, 38] is expected for the two-dimensional manifolds giving values of $\mu = 0.25$ and $\mu \sim 0.5 - 0.6$, respectively, for the dynamical exponent μ in these scenarios [55]. We note that random bond disorder exponents have been confirmed by measurements of domain wall creep and roughness in an ultrathin magnetic film [17]. In a random field scenario, in which defects locally asymmetricize the ferroelectric double well potential, $\zeta = \frac{4-d}{3}$ [39], giving $\mu = 1$ for all dimensionalities of the manifold between 1 and 4.

L_c is also the length scale at which pinning appears in the system in the presence of a driving force. Using [56] (5) for $u \sim \xi$ and $L = L_c$ one can directly obtain [57] the critical field E_c

$$E_c \simeq \frac{\sigma_w \xi}{P_s} \left(\frac{1}{L_c}\right)^2 \quad (9)$$

For driving forces above the critical force f_c , the interface is unpinned even at zero temperatures since the force is large enough to overcome the pinning barriers. For $f \ll f_c$, however, the force is not large enough to overcome the barriers and the motion proceeds by thermal activation. This is the creep regime, leading to a small and non-linear response. In our case, a rough estimate of the values of E_c may thus be obtained by extrapolating the linear behavior of the velocity, which occurs at high field values. Although we were unable to extend our measurement significantly into this region, we can nonetheless at least place a lower bound on the value of E_c of 180 MV/m, as indicated on Fig. 11 for one of our thinner films, where higher values of the field could be implemented. Taking ξ to be of the order of a unit cell, we can use the field data to extract an approximate value of $L_c \sim 0.2$ nm, below the limit of resolution of our measurement.

In the creep regime, we can rewrite (5). For simplicity we write formulas for the isotropic case. Using the scaling $u \sim \xi(L/L_c)^\zeta$ one obtains

$$E(u, L) = U_c \left(\frac{L}{L_c}\right)^{d-2+2\zeta} - 2P_s E L_c^d \xi \left(\frac{L}{L_c}\right)^{d+\zeta} \quad (10)$$

where $U_c = \sigma_w \xi^2 L_c^{d-2}$. Minimizing the energy with respect to the external field E , we obtain the size of the

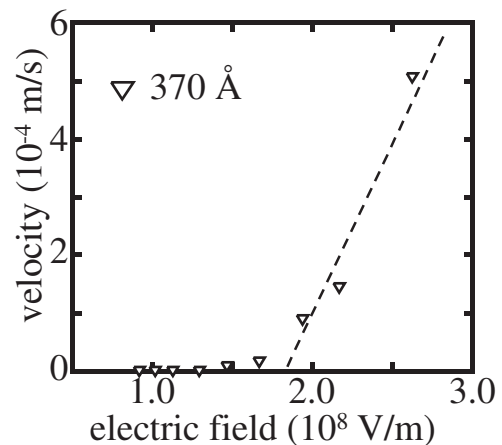


FIG. 11: Domain wall velocity as a function of the applied electric field in a 37 nm film. Extrapolating the linear behavior at high fields allows the critical field E_c to be estimated as 100 MV/m.

minimal nucleus capable of moving to a lower energy state as

$$L_{creep}/L_c = (f_c/f)^{1/(2-\zeta)} \quad (11)$$

with $f = 2P_s E$. The minimal barrier height to be passed by thermal activation thus corresponds to the length L^* , leading to a velocity of the form

$$v \propto \exp(-\beta U_c (f_c/f)^{\frac{d-2+2\zeta}{2-\zeta}}) \quad (12)$$

if one assumes an Arrhenius law in passing the barriers. The very slow (creep) response is due to the fact that for a small force the system would have to rearrange large portions of the interface to be able to find a new metastable state of low enough energy. The barriers a domain wall must pass to make such a rearrangement therefore diverge as the force goes to zero. This divergence could inherently explain the very high stability of domain structures we have observed in our films, in the limit of zero electric fields, even at relatively high temperatures.

The expression (11) gives the critical nucleus size L_{creep} as a function of the applied field E and L_c . We note that this expression is independent of the dimensionality of the film, and that the applied and critical fields are present as a ratio, thus removing the uncertainty associated with the correction of the field in the AFM tip-ferroelectric thin film configuration. As for the case of the periodic potential, these expressions are valid if the size of the nucleus is smaller than the thickness of the sample. Otherwise one of the dimensions of the nucleus should be replaced by the thickness, transforming a two-dimensional interface into a one-dimensional line. A crucial difference between the periodic and the disordered cases is that creep due to disorder can still exist in the one-dimensional situation, contrary to the periodic case. Note that the question of whether the films

should be considered as one- or two-dimensional depends on which mechanism controls the nucleus. A film could thus be in the one-dimensional limit for the periodic potential, thereby invalidating the periodic potential as a possible origin for the creep process, and still be in the two-dimensional limit for the disorder provided that the size of the nucleus due to disorder remains smaller than the thickness of the film. Although creep is still present in the one-dimensional disordered case, the value of the exponent μ depends on the dimension. Using the values for E_c and L_c we had obtained, we can estimate the size of the critical nucleus for the creep process and compare it with that found for the Miller-Weinreich formulation. In our system, the applied field is a function of the distance r away from the tip center. Using the largest possible (random field) value of ζ we find L_{creep} to vary between 0.2 and 1 nm in the thinnest films (29.0 – 51.0 nm), and 0.2 and 2.5 nm in the thickest films (95.0 – 130.0 nm). Note that in all cases $L_{creep} \sim 0.01r$, where r is the radius of the domain, so the approximation of a linear domain wall is quite reasonable at that scale +[58].

Interestingly, the anomalously large size of the nucleus given by the Miller-Weinreich model has previously been remarked on by Landauer [40]. Moreover, studies of the piezoelectric effect and dielectric permittivity in PZT films [41, 42] have shown non-linear features which cannot be described by a simple phenomenological model, but which could be described by the pinning of domain walls at randomly distributed pinning centers.[59] The scenario of weak pinning of elastic interfaces in disordered media was also invoked as a possible explanation for the dielectric dispersion observed in the ferroelectric RbH_2PO_4 [43]. The present study, investigating the static and dynamic behavior of individual ferroelectric domains with nanoscale resolution therefore provides an important clarification of this issue from the microscopic point of view.

VI. DOMAIN WALL DYNAMICS IN THE PRESENCE OF ARTIFICIAL DEFECTS

Another way to approach the question of ferroelectric domain wall creep, and its microscopic origins, is to investigate the effects of changing the disorder in the film. We studied two different types of defects: columnar tracks of amorphous material introduced by heavy ion irradiation (carried out by C. Simon and A. Ruyter at GANIL), and planar a-axis oriented inclusions introduced in thicker films during growth. For the irradiated films, samples 51.0 to 116.0 nm thick were half-shielded by metallic plates before irradiation, in order to directly compare domain dynamics in non-irradiated and irradiated regions of the same sample. As shown in the AFM topography scan in Fig. 12(a), the tracks are 6 – 13 nm in diameter at the point of entry, and appear as small white “bumps”, since the amorphous material is less dense than the crystalline form surrounding the tracks. As shown

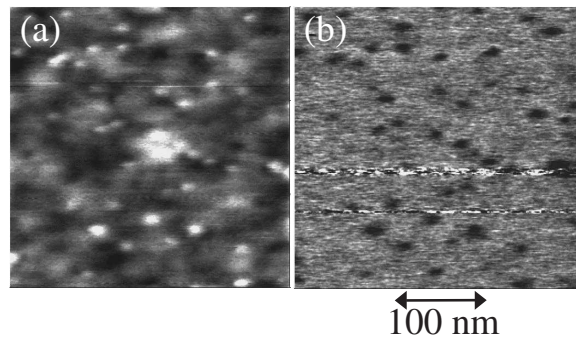


FIG. 12: Topography (a) and PFM (b) measurements of a 95.4 nm sample with columnar defects created by heavy ion (Pb) irradiation. On the film surface, the defects appear as white “bumps” in the topography, corresponding to the dark contrast regions in the PFM image, which we were unable to switch to the uniform polarization of the background.

in the corresponding piezoresponse image (Fig. 12(b)), these are exactly the regions which remain unaffected by attempts to uniformly polarize the area by scanning with a constant negative voltage, appearing as dots with dark phase contrast, as opposed to the lighter phase contrast of the rest of the image. Thus, irradiation defects can be distinguished from merely topographic features like the large white “bump” in the middle of the topographical scan, which switches under the application of an electric field and does not appear as a corresponding dark area in the piezoresponse image. The density of defects observed in this image ($4.7 \times 10^{10} / \text{cm}^2$) agrees reasonably with the nominal irradiation density $4 \times 10^{10} / \text{cm}^2$ used, considering the small area ($300 \times 300 \text{ nm}^2$) over which the Poisson distribution is observed. To ensure continuous tracks throughout the sample, with the ions lodging deep in the substrate, measurements from other experiments on similar oxides carried out at GANIL were used to determine irradiation energies [44]. To produce the planar a-axis inclusion, we grew relatively thick films, slightly varying the temperature from its optimal range, which generally results in the presence of a-axis, as shown in the AFM topography (Fig. 13(a)). Once again, the a-axis oriented regions do not respond to switching attempts, as shown in the piezoresponse image in Fig. 13(b), since the applied field is perpendicular to the polarization axis. These defects are approximately 25 nm wide, extending for hundreds of nanometers in the crystallographic a and b axis directions, and inclined at 45° to the c-axis of the film [45]. In all films, 25 domain arrays were written, and the domain dynamics extracted as described previously [27]. In the a-axis films, domains were written adjacent to, but not right on top of the a-axis inclusions.

As shown in Fig. 14(a) for a 95.4 nm film, we find that domain sizes are comparable in both the irradiated and normal regions of the sample. However, for longer writing times, domains in the irradiated part of the sample appear somewhat larger than those written in the normal regions of the same sample. When comparing pure

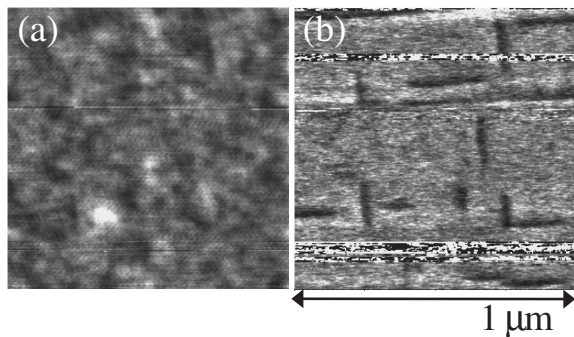


FIG. 13: Topography (a) and PFM (b) measurements of a 108.9 nm sample with a-axis inclusions. These appear as criss-crossing lines on the surface, parallel to the a and b crystallographic axes of the film. Since the direction of the polarization is in plane, these regions do not switch when a perpendicular electric field E is applied across the film, once again appearing as dark contrast lines against a uniformly polarized background.

c-axis film 95.4 and 130.0 nm thick to a film of similar thickness (108.9 nm) with a-axis inclusions (Fig. 14(b)) this increase in domain size for longer writing times in the presence of defects is also observed. The effect of the irradiation tracks and a-axis inclusions becomes more evident when the Arrhenius plot of velocity vs the inverse field is compared for the same films (Fig. 15(a) and (b)). We find a decrease in the values of the dynamical exponent in the irradiated regions, as compared to the normal regions, from a range of 0.62 – 0.69 to one of 0.38 – 0.5. This decrease is even more marked for films containing a-axis inclusions, with μ values of 0.31 and 0.19 [20]. That this is not a thickness effect can be seen by comparing the a-axis-containing films to pure c-axis films of similar thickness, in which μ values of 0.69 and 0.78 (for 95.4 and 130.0 nm thick films, respectively) are observed. It is interesting to note that both these types of defects are large compared to the thickness of the wall itself, occur at a relatively low density, and are either columnar or planar, as opposed to point-like. The mechanism by which they affect the dynamics of the domain wall is therefore unlikely to be a direct weak collective pinning effect, and thus the marked decrease observed in the dynamical exponent is somewhat surprising. Possibly, the relaxation of strain in the film caused by these macroscopic “defects” changes the density or pinning force of the inherent, weak point defects present in the film, thus affecting the disorder potential experienced by the domain wall. Since a large amount of energy is dissipated within the substrate by the heavy ion during irradiation, with possible deformation as strain induced in the substrate [46, 47], this could result in additional strain effects on the ferroelectric film. Alternatively, the presence of defects which penetrate through the entire thickness of the film might act to make the wall more rigid – and therefore more one-dimensional. A more detailed investigation of domain walls in the presence of these defects,

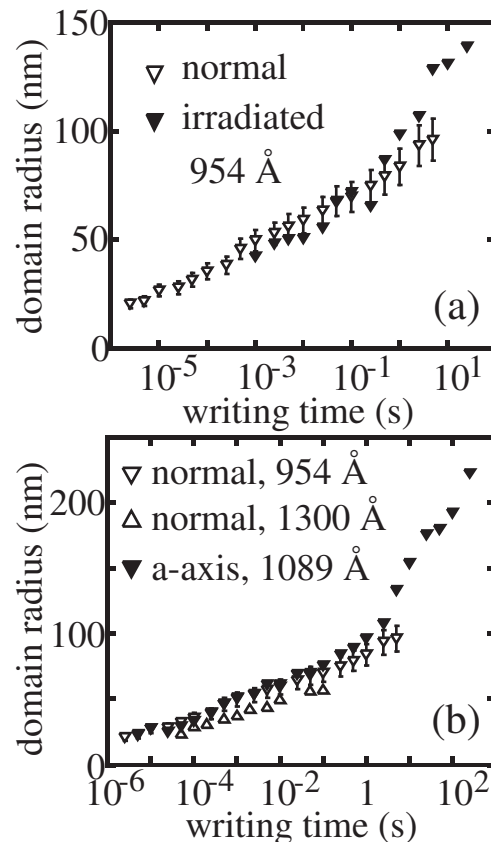


FIG. 14: Domain radius as a function of the writing time for the 95.4 nm half-irradiated film (a), and for the 108.9 nm film with a-axis inclusion (b). In both cases, the domains written with longer writing times appear larger than in the non-irradiated or pure c-axis films included as a comparison.

perhaps looking at their specific individual interaction, is needed to ascertain the microscopic nature of this behavior.

VII. CONCLUSION

Using the unprecedented control and precision provided by AFM, we were able to study the growth of individual nanoscale ferroelectric domains in epitaxial thin films, investigating both the fundamental physics of domain wall motion, and its consequences for possible AFM-ferroelectric applications. Our studies demonstrate that domain wall motion in ferroelectric thin films is a creep process in which $v \propto \exp(-\beta U_c (E_c/E)^\mu)$, with a dynamical exponent μ between ~ 0.7 and 1.0. This process controls the lateral growth of domains in low electric fields applied by an AFM tip. A detailed analysis of the possible microscopic origins of the observed domain wall creep suggests that it is the result of competition between elastic behavior and pinning in a disorder potential. The reduced dimensionality of our thin films compared to the size of the critical nucleus precludes pinning in the com-

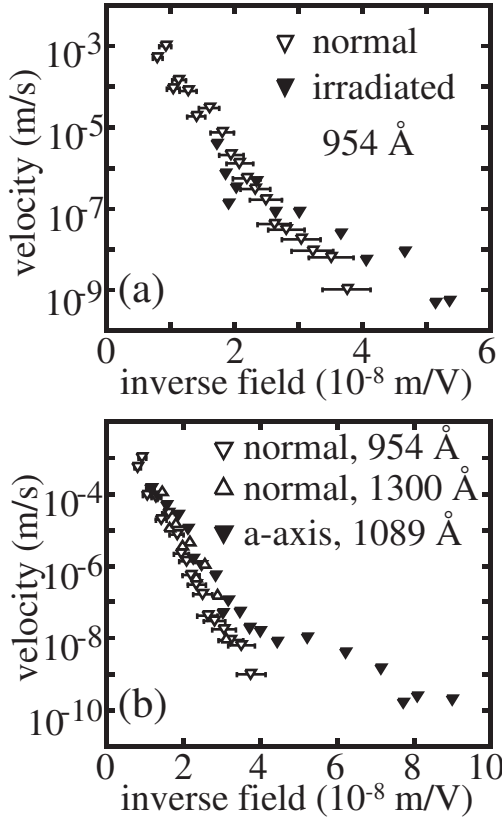


FIG. 15: Domain wall speed as a function of the inverse applied field for the films shown in Fig. 14. In the presence of defects, the values of the creep exponent μ decrease from 0.69 to 0.38 and from 0.69 and 0.78 to 0.31 in the half-irradiated film, and the pure c-axis films vs the film with a-axis inclusions, respectively.

measure the potential of the crystal itself as the mechanism for the non-linear field dependence of the velocity. We have also observed that the presence of artificially introduced defects, such as irradiation tracks or a-axis inclusions, strongly decreases the dynamical exponent for domain wall creep, from $\sim 0.6 - 0.7$ to $0.4 - 0.5$ and ~ 0.31 . All the domains show high stability (up to 4 months for the longest duration experiments), inherently explained by the physics of a system in which elasticity and pinning by a disorder potential compete, leading to glassy behavior in the presence of low electric fields. This high stability is important for applications such as information storage or surface acoustic wave devices based on ferroelectric domain structures. Our studies have also identified the key parameters controlling domain size as the writing time, the applied voltage, and the confinement of the electric field, with encouraging results for novel tip geometries using carbon nanotube bundles.

Acknowledgments

The authors would like to thank M. Dawber and C. H. Ahn for enriching discussions. Special thanks to D. Chablaix for useful technical developments and to S. Brown for careful reading of the manuscript. This work was supported by the Swiss National Science Foundation through the National Center of Competence in Research “Materials with Novel Electronic Properties-MaNEP” and Division II. Further support was provided by the New Energy and Industrial Technology Development Organization (NEDO) and the European Science Foundation (THIOX).

-
- [1] K. M. Larkin, G. R. Kline, and T. McCarron, IEEE Trans. Microwave Theory Tech. **43**, 2933 (1995).
- [2] J. F. Scott and C. A. Araujo, Science **246**, 1400 (1989).
- [3] R. Waser and A. Rüdiger, Nature Mater. **3**, 81 (2004).
- [4] T. Ohnishi, D. Komiyama, T. Koida, S. Ohashi, C. Stauter, H. Koinuma, A. Ohtomo, M. Lippmaa, N. Nakagawa, M. Kawasaki, T. Kikuchi, and K. Omote, Appl. Phys. Lett. **79**, 536 (2001).
- [5] A. Lin, X. Hong, V. Wood, A. A. Verevkin, C. H. Ahn, R. A. McKee, F. J. Walker, and E. D. Specht, Appl. Phys. Lett. **78**, 2034 (2001).
- [6] M. Lippmaa, K. Terai, N. Nakagawa, K. Shibuya, M. Kawasaki, and H. Koinuma, Proc. SPIE Int. Soc. Opt. Eng. **4467**, 128 (2001).
- [7] G. Asano, H. Morioka, H. Funakubo, T. Shibutarni, and N. Oshima, Appl. Phys. Lett. **83**, 5506 (2003).
- [8] T. Hidaka, T. Maruyama, M. Saitoh, N. Mikoshiba, M. Shimizu, T. Shiosaki, L. A. Wills, R. Hiskes, S. A. Discarolis, and J. Amano, Appl. Phys. Lett. **68**, 2358 (1996).
- [9] T. Tybell, C. H. Ahn, and J.-M. Triscone, Appl. Phys. Lett. **72**, 1454 (1998).
- [10] A. Gruverman, Appl. Phys. Lett. **75**, 1452 (1999).
- [11] P. W. Anderson and Y. B. Kim, Rev. Mod. Phys. **36**, 39 (1964).
- [12] R. C. Miller and G. Weinreich, Phys. Rev. **117**, 1460 (1960).
- [13] G. Blatter, M. V. Feigel'man, V. B. Geshkenbein, A. I. Larkin, and V. M. Vinokur, Rev. Mod. Phys. **66**, 1125 (1994).
- [14] L. B. Ioffe and V. M. Vinokur, J. Phys. C **20**, 6149 (1987).
- [15] T. Nattermann, Europhys. Lett. **4**, 1241 (1987).
- [16] P. Chauve, T. Giamarchi, and P. Le Doussal, Phys. Rev. B **62**, 6241 (2000).
- [17] S. Lemerle, J. Ferré, C. Chappert, V. Mathet, T. Giamarchi, and P. Le Doussal, Phys. Rev. Lett. **80**, 849 (1998).
- [18] P. Kim, Z. Yao, C. A. Bolle, and C. M. Lieber, Phys. Rev. B **60**, R12589 (1999).
- [19] D. T. Fuchs, E. Zeldov, T. Tamegai, S. Ooi, M. Rappaport, and H. Shtrikman, Phys. Rev. Lett. **80**, 4971 (1998).
- [20] P. Paruch, T. Giamarchi, and J.-M. Triscone, Ann. der Phys. **13**, 95 (2004).
- [21] A. K. S. Kumar, P. Paruch, J. M. Triscone, W. Daniau, S. Ballandras, L. Pellegrino, D. Marré, and T. Tybell, Appl. Phys. Lett. **85**, 1757 (2004).
- [22] P. Paruch, T. Tybell, and J.-M. Triscone, Proc. 10th International Ceramics Congress CIMTEC 2002 675 (2002).
- [23] P. Paruch, T. Tybell, and J.-M. Triscone, Appl. Phys. Lett. **79**, 530 (2004).
- [24] Y. Cho, K. Fujimoto, Y. Hiranaga, Y. Wagatsuma, A. Onoe, K. Terabe, and K. Kitamura, Appl. Phys. Lett. **81**, 4401 (2002).
- [25] J. Li, B. Nagaraj, H. Liang, W. Cao, C. H. Lee, and R. Ramesh, Appl. Phys. Lett. **84**, 1174 (2004).
- [26] V. Wood, X. Hong, and C. H. Ahn, 2001, private communication.
- [27] T. Tybell, P. Paruch, T. Giamarchi, and J.-M. Triscone, Phys. Rev. Lett. **89**, 097601 (2002).
- [28] W. J. Merz, Phys. Rev. **95**, 690 (1954).
- [29] F. Fatuzzo and W. J. Merz, Phys. Rev. **116**, 61 (1959).
- [30] B. Meyer and D. Vanderbilt, Phys. Rev. B **65**, 104111 (2002).
- [31] T. Emig and T. Nattermann, Eur. Phys. J. B **8**, 525 (1999).
- [32] A. I. Larkin, Sov. Phys. JETP **31**, 784 (1970).
- [33] A. I. Larkin and Y. N. Ovchinnikov, J. Low Temp. Phys **34**, 409 (1979).
- [34] D. A. Huse and C. L. Henley, Phys. Rev. Lett. **54**, 2708 (1985).
- [35] M. Kardar and D. R. Nelson, Phys. Rev. Lett. **55**, 1157 (1985).
- [36] D. A. Huse, C. L. Henley, and D. S. Fisher, Phys. Rev. Lett. **55**, 2924 (1985).
- [37] D. E. Wolf and J. Kertész, Europhys. Lett. **4**, 651 (1987).
- [38] B. M. Forrest and L. H. Tang, Phys. Rev. Lett. **64**, 1405 (1990).
- [39] D. S. Fisher, Phys. Rev. Lett. **56**, 1964 (1986).
- [40] R. Landauer, J. Appl. Phys. **28**, 227 (1957).
- [41] D. Damjanovic, Phys. Rev. B **55**, R649 (1997).
- [42] D. V. Taylor and D. Damjanovic, Appl. Phys. Lett. **73**, 2045 (1998).
- [43] V. Mueller, Y. Shchur, H. Beige, S. Mattauich, J. Glinne-mann, and G. Heger, Phys. Rev. B **65**, 134102 (2002).
- [44] V. Hardy, A. Ruyter, J. Provost, D. Groult, and C. Simon, Physica C **224**, 143 (1994).
- [45] T. Tybell, C. H. Ahn, and M. F. J.-M. Triscone, Proceedings of the 11th IEEE International Symposium on the Applications of Ferroelectrics 431 (1998).
- [46] B. Hensel, B. Roas, S. Henke, R. Hopfengärtner, M. Lippert, J. P. Ströbel, M. Vidić, G. Saemann-Ischenko, and S. Klaumünzer, Phys. Rev. B **42**, 4135 (1990).
- [47] M. Konczykowski, 2004, private communication.
- [48] We note that during AFM writing, the exact magnitude of the effective field is difficult to quantify, because of a possible gap between the film surface and the tip [8], and variations in tip shape. Local piezoelectric hysteresis measurements on 120Å- 800Å thick films show that the minimum switching field is $\sim 6-16$ times larger than the bulk coercive field, an effect that is not observed with macroscopic electrodes on the similar films. The effective field E in the experiments is therefore presumably \sim one order of magnitude smaller than that calculated as $E(r)$ in this study. This has no effect on the exponent μ governing the exponential velocity dependence. Unless otherwise noted, the values reported are the directly calculated ones, with no further corrections.
- [49] In the absence of a depolarization field the nucleus is isotropic. Taking into account the depolarization changes the shape of the nucleus, but does not affect in an essential way the physics leading to the creep process.
- [50] This value is computed for PbTiO₃. The presence of Zr in PZT would lead to local variations of this energy density.
- [51] There are constants of order one, dependent on the dimension d , which have been omitted from each term in the energy. These constants will not affect the creep exponent μ .
- [52] Note that in order to take into account the depolarization effects lengths along the vertical axis have to be scaled by a factor $(\sigma_p/\sigma_w)^{1/2}$, as in (4). Here L denotes lengths perpendicular to the polarization direction.

- [53] In this simplified description we assume that the temperature is small enough to neglect thermal effects.
- [54] Above L_c , the domain wall can also remain locally pinned on individual strong pinning sites, but in the present discussion, only weak collective pinning is considered.
- [55] For the random bond case, long range dipolar forces would push in the two dimensional case the exponent to $\mu \sim 0.66$ [31]
- [56] We now denote simply by ξ the $\max(\xi, r_f)$.
- [57] As before the length here is the length perpendicular to the polarization direction.
- [58] In the thinnest films, longer writing times resulted in un-
- stable and destructive interactions between the tip and the sample. Therefore the larger domains obtained for long writing times were only measured in the thicker films.
- [59] We note that the studies referred to were carried out in thick (over $1 \mu\text{m}$) ceramic and sol-gel films, where the presence of multiple grain boundaries and differently oriented domain walls provides a much more complex disorder landscape compared to the epitaxially grown films used for this study.